Proton stopping in dense molecular hydrogen: A molecular-confinement model

S. A. Cruz,[1,2,*] J. Soullard,[3] and E. G. Gamaly[2]
[1]*Programa de Simulación Molecular, Instituto Mexicano del Petroleo, Apartado Postal 14-805, 07730 México, Distrito Federal, Mexico*
[2]*Departamento de Física, Universidad Autónoma Metropolitana-Iztapalapa, Apartado Postal 55-534, 09340 México, Distrito Federal, Mexico*
[3]*Instituto de Física, Universidad Nacional Autónoma de México, Apartado Postal 20-364, 01000 México, Distrito Federal, Mexico*
(Received 29 April 1999)

A molecular-confinement model is proposed for the calculation of density effects on the electronic stopping cross section (S_e) in a condensed medium. In this model, the collective intermolecular interactions in the medium are represented by a mean field in which a particular molecule is embedded including the spatial constrictions imposed by the surrounding molecules. A molecule is thus viewed as a caged-in system within a spherical boundary with finite potential barrier height V_B. Changes in the molecular electronic properties and molecular conformation as a function of medium density are self-consistently treated. As a first example of a general treatment for more complicated target structures, the model is explicitly applied to the case of proton stopping in dense molecular hydrogen. The lowest barrier height ($V_B=0$) was selected for the stopping calculations since it provides a more realistic pressure-density relation at $T=0$ K than higher barrier values. Our results for dense molecular hydrogen predict a very small to moderate reduction in S_e relative to the gas phase in going from atmospheric pressure (0.036 mol/cm^3, $\Delta S_e \approx 0.5\%$) up to 136 GPa (0.380 mol/cm^3, $\Delta S_e \approx 24\%$) for either the liquid or solid phase as determined by the phase diagram for this medium. [S1050-2947(99)08609-6]

PACS number(s): 34.50.Bw, 34.10.+x, 62.50.+p, 61.80.Az

I. INTRODUCTION

The outcome of more accurate experimental techniques to measure electronic stopping cross sections (S_e) in compound materials has provided evidence on important deviations from Bragg's additivity rule as well as on target physical phase state effects on S_e [1–7]. Chemical binding effects due to the target molecular structure have been considered by the theory through various models with reasonable success [7,8–16]. These models, however, are designed on the basis of the free-molecule properties and are more suitable for the treatment of targets in the gas phase. For a condensed medium—like a molecular liquid or solid—the short intermolecular distances and corresponding interactions may have a significant effect on the electronic and structural properties of the constituent molecules as compared to the gas phase, giving rise to the observed changes in the stopping cross section for different physical states of the target. Previous ideas to model this situation have been put forward by other authors [17,18], who considered the state of aggregation of the medium in terms of the spatial confinement imposed on the electronic distribution of each molecule due to its surrounding neighbors and using Lindhard's theory in the local-density approximation [19]. In these models, spatial confinement is viewed as a boxed-in molecule within hard walls, whereby the redistribution of the total molecular electronic density is evaluated as the sum of the free-atom densities of its atomic constituents, renormalized within the confinement volume. However, this perturbation approximation might not be valid for all confinement conditions—i.e., varying density within the same phase—since a redistribution of the electronic cloud must be accompanied by nuclear position relaxation. Furthermore, according to studies on small confined molecules [20–24], the electronic energy levels have a strong dependence on both the size of the confining box and the height of the potential barrier at the wall. Hence, mean excitation energies and stopping cross sections should be accordingly affected. In view of the above, we may deem that phase and molecular structure are intimately related and should influence simultaneously the outcome of an experimental determination of S_e.

The aim of this work is to present a model of molecular confinement by a penetrable barrier designed to describe the target properties in a given phase under different density conditions in order to analyze target-density effects on S_e. The case of proton stopping in dense molecular hydrogen is explicitly considered.

In the model proposed here, a given constituent molecule in a condensed medium is viewed as a caged-in system within a spherical boundary with finite potential barrier height V_B (padded spherical confining box). The height of the potential barrier corresponds physically to the mean field where a particular molecule is embedded and represents a measure of the confining capacity of the medium. On the other hand, the density of the medium establishes the degree of spatial constriction on the molecular electronic distribution. Hence, the barrier potential height as well as the confining volume may have consequent changes in the total electronic energy, internuclear distances, and mean excitation energy.

*Author to whom correspondence should be addressed. Address correspondence to Programa de Simulación Molecular, Instituto Mexicano del Petroleo, Apartado Postal 14-805, 07730, México, D.F., Mexico. Electronic address: scruz@www.imp.mx

Both the electronic structure and molecular conformation within different confining volumes are self-consistently treated. To this end we use the floating spherical Gaussian orbitals (FSGO) representation for the target molecular orbitals [25] and develop an *ab initio* calculation of the molecular ground-state energy and structure—hence allowing for electronic and nuclear redistribution—as a function of volume for the padded spherical confining box. The electronic density of the confined molecule is then incorporated into the orbital local plasma approximation (OLPA)/FSGO implementation of the kinetic theory [16] in order to account consistently for both density and chemical bonding effects in the stopping process. In Sec. II, a brief description of the molecular confinement model proposed here is discussed first on a general basis and then applied explicitly to the hydrogen molecule. Some relevant physical aspects of this boxed-in system are pointed out here including its predictions for the pressure-density dependence of liquid molecular hydrogen at $T=0$ K. Section III deals with the calculation of the proton electronic stopping cross section for different compression states of molecular hydrogen. Finally, in Sec. IV, a discussion and the conclusions of this work are presented. Atomic units are used throughout this work unless otherwise indicated.

II. MOLECULAR CONFINEMENT MODEL

A. General strategy

According to Frost [25]—in the FSGO approach—each electron pair in a given core, bond, or lone-pair orbital within a free molecule in its ground state may be represented by a localized molecular orbital as a single floating Gaussian:

$$\psi_k(\mathbf{r}-\mathbf{R}_k)=(2/\pi\sigma_k^2)^{3/4}e^{-(\mathbf{r}-\mathbf{R}_k)^2/\sigma_k^2}, \tag{1}$$

where σ_k is the orbital radius and $\mathbf{R}_k$ the position of its center and are obtained after total-energy minimization for the molecular Hamiltonian.

For a boxed-in molecule, let V_c define a confining volume for our system limited by a boundary $S(\mathbf{r}_B)$, where $\mathbf{r}_B$ is the position vector of any point on the boundary relative to the origin. Let us further assume the barrier height at the boundary has a constant finite value, V_B, hence the confining potential has the form

$$V(\mathbf{r})=\begin{cases}0 & (\mathbf{r}\in V_c)\\ V_B & (\mathbf{r}\notin V_c),\end{cases} \tag{2}$$

where $\mathbf{r}$ denotes the position of any electron relative to the origin.

Clearly, inclusion of the function $V(r)$ in the molecular Hamiltonian demands different expressions for the interior (Ψ_k^i) and exterior (Ψ_k^o) representation of a localized orbital such that boundary continuity conditions and normalization are satisfied. With these conditions and in the spirit of the FSGO representation, we propose for a localized orbital of a molecule under confinement the following ansatz for the interior and exterior representations:

$$\Psi_k^i(\mathbf{r}-\mathbf{R}_k)=N_k^i[e^{-a_k(\mathbf{r}-\mathbf{R}_k)^2}-e^{-b_k(\mathbf{r}_B-\mathbf{R}_k)^2}] \quad (\mathbf{r}\in V_c), \tag{3a}$$

$$\Psi_k^o(\mathbf{r}-\mathbf{R}_k)=N_k^o e^{-g_k(\mathbf{r}-\mathbf{R}_k)^2} \quad (\mathbf{r}\notin V_c), \tag{3b}$$

where the parameters a_k, b_k, g_k and the normalizing factors N_k^i, N_k^o are related through the boundary and normalization conditions.

Following Frost, for the set $\{\Psi_i\}$ of nonorthogonal orbitals given by Eqs. (3a) and (3b), if $\mathbf{S}$ is the overlap matrix of the set and $\mathbf{T}=\mathbf{S}^{-1}$ its inverse, then the electronic energy for the molecule is

$$E=2\sum_{j,k}(j|k)T_{jk}+\sum_{k,l,p,q}(kl|pq)[2T_{kl}T_{pq}-T_{kq}T_{lp}], \tag{4}$$

where $(j|k)$ are the one-electron integrals and $(kl|pq)$ the two-electron Coulomb and exchange terms given by

$$(j|k)=\int_\Gamma \Psi_j h\Psi_k\, d\nu, \tag{5a}$$

$$(kl|pq)=\int_\Gamma \Psi_k(1)\Psi_l(1)r_{12}^{-1}\Psi_p(2)\Psi_q(2)\, d\nu_1 d\nu_2, \tag{5b}$$

with

$$h=-\tfrac{1}{2}\boldsymbol{\nabla}^2-\sum_\nu \frac{Z_\nu}{r_\nu}+V(\mathbf{r}). \tag{5c}$$

The first term in Eq. (5c) corresponds to the one-electron kinetic energy operator and the second one to the electron-nuclear attraction for a system with ν nuclei of charge Z_ν. $V(\mathbf{r})$ is the confining potential given by Eq. (2) and r_{12} is the electron-electron relative distance. Note that the symbol Γ in the above expressions indicates in a generic way the domain of integration, which is different for the interior and exterior wave functions.

In general, the total energy W will be a function of the orbital parameters (a_k, b_k, g_k), orbital positions $(\mathbf{R}_k)$, nuclear positions $(\mathbf{r}_\nu)$, volume of confinement (V_c), and barrier height (V_B), i.e.,

$$W(a_k,b_k,g_k,R_k,r_\nu,V_c,V_B)=E(a_k,b_k,g_k,R_k,r_\nu,V_c,V_B)+\sum_{\mu<\nu}\frac{Z_\mu Z_\nu}{r_{\mu\nu}}, \tag{6}$$

where E is given by Eq. (4) and the second term is the internuclear repulsion. For a given confinement volume and barrier height, energy minimization relative to all quantities $(a_k, b_k, g_k, \mathbf{R}_k, \mathbf{r}_\nu)$ provides the parameters defining the corresponding molecular configuration.

B. Application to the hydrogen molecule

We now focus our attention on a hydrogen molecule in its ground state confined by a penetrable spherical cage of radius R_c. Within the FSGO model, this two-electron system is represented by a single Gaussian orbital centered at the origin [$\mathbf{R}_k=\mathbf{0}$ in Eq. (1)]. According to Eqs. (3a) and (3b), putting $r_B=R_c$, the interior and exterior ansatz orbitals for this case are

$$\Psi^i(r)=N^i(e^{-ar^2}-e^{-bR_c^2}) \quad (r<R_c), \tag{7a}$$

$$\Psi^o(r)=N^o e^{-gr^2} \quad (r\geqslant R_c). \tag{7b}$$

Using boundary and normalization conditions, the following relations are obtained for the normalization factors and orbital parameters:

$$N^o=N^i[e^{(g-a)R_c^2}-e^{(g-b)R_c^2}], \tag{8a}$$

$$g=a/[1-e^{(a-b)R_c^2}], \tag{8b}$$

hence only two orbital parameters are independently optimized.

Using Eqs. (7) and (8), and since only one FSGO is required, the overlap matrix is a scalar ($S=1$) and the evaluation of Eqs. (4)–(6) for this two-nuclei problem may be easily done analytically. However, the final expressions become too long to be shown here. We simply state here that after global minimization of the total energy (W) [Eq. (6)] for a given box radius (R_c) and barrier height (V_B), the corresponding optimum values for the orbital parameters (a,b) and half internuclear distances (R_n) are obtained. Note from Eq. (2) that if $V_B=\infty$ (hard wall), the wave function must vanish outside the confining volume. This is achieved setting $a=b$ ($g\rightarrow\infty$) in Eq. (8b). On the other hand, if $V_B=0$ (''transparent'' soft wall), the interior and exterior wave functions are the same, hence from Eq. (8b), $b\rightarrow\infty$ and $a=g$. For these two extreme cases we only require one orbital parameter. The corresponding explicit expressions for the relevant, one- and two-electron integrals are given in the Appendix.

Before proceeding to the stopping power calculations, it is worthwhile to briefly analyze and validate the results of the confinement model proposed here. To the authors' knowledge, there are no similar studies in the literature for the H_2 molecule confined within soft boxes. However, we can compare our results for the hard-wall case with other more sophisticated treatments in order to gain some confidence in our results. LeSar and Herschbach [21] studied the hydrogen molecule confined within spheroidal hard boxes using a variational calculation with a five-term James-Coolidge wave function [26]. Interestingly enough, the aforementioned authors find that the symmetry of the confining boxes for which the total energy is a minimum is practically spherical for all box sizes. This allows proper comparison with our spherically confined molecule. Moreover, recent exact calculations for hard-wall spheroidal confinement of H_2 by Pang [24] using a diffusion quantum Monte Carlo method show an agreement within 1% difference with the corresponding variational results by LeSar and Herschbach. Hence it is sufficient to compare with the results of the latter authors.

Figure 1 shows a plot of the total energy against the confining box radius for the two extreme values of the barrier height: $V_B=0$ and $V_B=\infty$. For the hard-wall case we observe that our energy values (continuous curve) are systematically above those of LeSar and Herschbach (solid circles) following the same qualitative behavior as a function of box radius. For small box radii ($R_c<2a_0$) both calculations merge together to coalesce into the well-known particle-in-a-box result. Note the different energy dependence for the ''transparent''-soft-wall case. Here, in contrast with the hard-wall model, a less pronounced variation of the electronic energies as the box radius decreases is observed, in agreement with other calculations performed for the H_2^+ molecular ion [22]. Interestingly enough, this model predicts a threshold box radius ($R_c\approx 1.25a_0$) below which no bound state for H_2 is available. This behavior is characteristic of the incomplete confinement of the electron cloud and renders a more realistic description of the pressure effects on the molecular properties of H_2 [27].

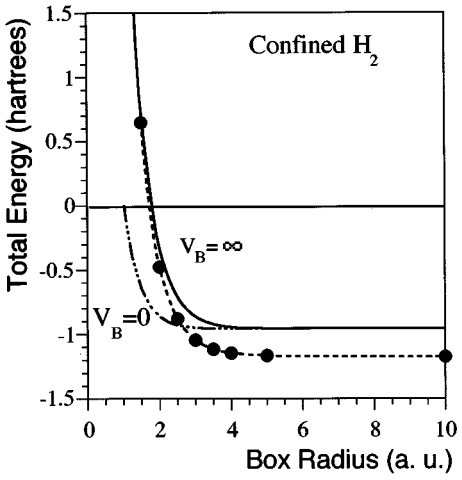

FIG. 1. Total ground-state energy of molecular hydrogen as a function of confinement radius for two extreme values of the confining barrier potential. ($V_B=\infty$): (——) this work; (●) ''exact'' calculations from Ref. [21]. ($V_B=0$): (---···---) this work. The dashed curve is drawn to guide the eye.

For completeness, in Table I the values of the total energy, internuclear distance ($R_e=2R_n$), and orbital parameter (a) are displayed for selected values of density for $V_B=0$ and $V_B=\infty$. The corresponding calculations by LeSar and Herschbach ($V_B=\infty$) are given within parentheses. Here we observe that our total-energy values are typically ≈20% above those of the latter authors (see Fig. 1). This quantitative difference is a consequence of the use of a single-Gaussian representation for the wave function. According to Moshinsky [28], this corresponds to the lowest-order (zero-quanta) expansion in terms of the harmonic-oscillator basis set and in this case total energy values are obtained ≈20% above the Hartree-Fock limit. The large discrepancy (40%) observed with the ''exact'' calculation for 0.333 mol/cm^3 ($R_c=2a_0$) may be a consequence of the onset (see Fig. 1) of a steeper change in the energy induced by the wall on the more compact Gaussian wave function. In spite of this, an overall fair agreement is observed with the calculations by LeSar and Herschbach for the internuclear distance as a function of box size. The later case reflects an important property of the FSGO model for molecular structure calculations [25]. In light of the above discussion, the same trend would be expected for the soft-wall case when compared with exact calculations when available. Here also a less pronounced variation of the internuclear distances as density increases are observed [22].

On the other hand, we may find the correlation between pressure and density for liquid molecular hydrogen under compression in order to make our treatment self-contained.

TABLE I. Density dependence of H_2 total energy, internuclear distance, and orbital parameter for zero and infinite confining potential barrier heights. Quantities in parentheses are corresponding values reported in Ref. [21].

Density (mol/cm^3)	Total energy W (hartrees)		Internuclear distance R_e (units of a_0)		Orbital parameter a (units of a_0^{-2})	
	$V_B=0$	$V_B=\infty$	$V_B=0$	$V_B=\infty$	$V_B=0$	$V_B=\infty$
0.333	−0.8617	−0.3331 (−0.4749)	1.251	0.944 (0.893)	0.44259	0.66504
0.171	−0.9309	−0.7117 (−0.8800)	1.367	1.112 (1.068)	0.37034	0.50807
0.099	−0.9509	−0.8613 (−1.0441)	1.438	1.248 (1.208)	0.33496	0.42151
0.062	−0.9552	−0.9216 (−1.1136)	1.466	1.348 (1.301)	0.32198	0.37131
0.042	−0.9558(7)	−0.9448 (−1.1440)	1.473	1.414 (1.355)	0.31907	0.34271
free molecule	−0.9559(4)	−0.9559(4) (−1.1716)	1.474	1.474 (1.403)	0.31865	0.31865

We stress at this stage that, since the confinement model only considers changes in the electronic ground-state energy and ignores rotational and translational motion inside the box, in this work we calculate the purely cold pressure which comes from changes in the total ground-state electronic energy relative to confinement volume, i.e., $P=-\partial W/\partial V_0$, where V_0 is the molecular volume associated to the density of the medium. Hence P is only comparable to pressure-density relations at absolute zero temperature. In what follows our reference to the pressure will be related exclusively to this cold pressure.

Figure 2(a) shows the pressure-density curves obtained in this work for the hard-wall (chain curve) and soft-wall (continuous curve) models. Full triangles represent the results from LeSar and Herschbach for their hard-wall model. Also shown is the 0-K isotherm (dashed curve) corresponding to a widely accepted equation of state (EOS) for fluid molecular hydrogen developed by Kerley [29]. Crosses represent the experimental EOS points for solid molecular hydrogen at 80 K from Evans and Silvera [30] and open diamonds correspond to a temperature-reduced (0 K) experimental EOS for the solid by Hemley *et al.* [31]. Clearly, the hard-wall model exaggerates the compression effect, whereas the soft-wall model gives a more realistic description, in agreement with similar results previously reported for the pressure effect on the H_2^+ molecular ion [22,23] and the helium atom [32]. The close correspondence between the real 0-K liquid and solid isotherms suggests a common intrinsic mechanism related to the electronic properties of the molecule. This observation might justify the use of the model proposed in this work for dense molecular hydrogen either in the liquid or solid phases at $T=0$ K. Perhaps the only difference we could distinguish in order to refer to one or another phase in our pressure-density calculations is the use of the Wigner-Seitz cell volume for the solid case and the effective molecular volume for the liquid just as we did in computing the curve shown in Fig. 2(a). Hence we will refer to dense hydrogen in a generic way keeping in mind that the physical existence of one or another phase must be defined by the associated pressure-temperature phase diagram. When necessary, thermal pressure may be estimated and added to the cold pressure as prescribed elsewhere [33–35]. However, this is beyond the scope of the present work.

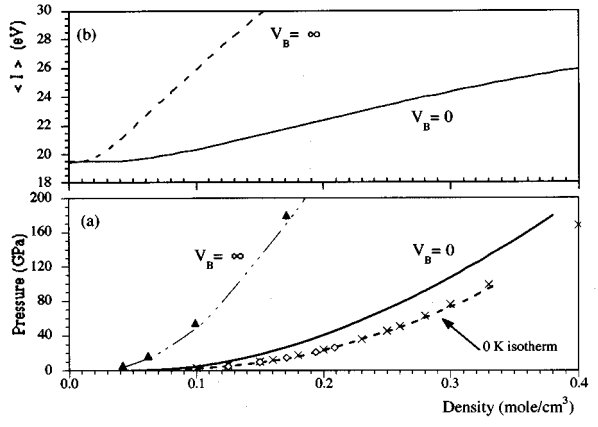

FIG. 2. (a) Pressure-density curves for H_2. Results of this work (---···---) and results from Ref. [21] (▲) for $V_B=\infty$. (——) this work for $V_B=0$ (see text). (---) 0 K isotherm for fluid H_2 [29], (×) experimental EOS points for solid H_2 at 80 K [30], (◇) temperature-reduced (0 K) experimental EOS for solid H_2 [31]. (b) Mean excitation energy, $\langle I\rangle$, for H_2 as a function of density for the two barrier potential heights indicated.

III. ELECTRONIC STOPPING CALCULATION

We now turn our attention to the treatment of the target-density effects on proton stopping in condensed molecular hydrogen. In order to apply the results obtained in the preceding section, we shall consider the projectile as penetrating a condensed medium where the intermolecular distances are small enough to create a potential barrier—due to the surrounding molecules—for the electrons associated to any particular molecule embedded in the medium. Furthermore, we assume for simplicity that the barrier height is constant and the medium is a liquid under different pressure conditions with consequent changes in density, which in turn are represented by different confinement box sizes. Our purpose is also to resort to a stopping model which fully incorporates the molecular electronic density properties. The orbital local plasma approximation implementation of the kinetic theory of stopping [36] has these properties and has shown its adequacy in the calculation of proton stopping cross sections in gaseous targets using FSGO [16]. The advantage in using this method lies in the possibility of adapting it for the case

of a condensed medium—as proposed in this work—and to make a consistent comparison with corresponding cross sections for the gas phase. We stress at this stage that the purpose of this work is to show the effect of target density on S_e when the target properties are properly modeled through molecular confinement. In this connection, any other method of calculation for S_e could be chosen as long as it incorporates the molecular properties of the target as described here.

In the frame of the OLPA/FSGO implementation of the kinetic theory, the orbital contribution to S_e may be obtained making use of the orbital decomposition scheme proposed by Oddershede and Sabin [37]. Within this spirit S_e becomes

$$S_e(v_1)=\sum_k S_{e,k}(v_1), \tag{9}$$

where $S_{e,k}$ is the contribution from orbital ''k'':

$$S_{e,k}(v_1)=\frac{4\pi e^4 Z_1^2 Z_2}{m v_1^2} L_k(v_1), \tag{10}$$

with m and e the electron mass and charge, respectively. Z_1 is the projectile nuclear charge, Z_2 is the total number of electrons of the molecular target, and L_k is the orbital stopping number, which in terms of the orbital mean excitation energy (I_k) and its electron population (ω_k) is given as [16]

$$L_k(v_1)=\pi v_1^2 Z_2^{-1}\omega_k \int_{\alpha_k}^{\infty} \ln\left[\frac{2mv'^2}{I_k}\right] dv' \times \int_0^{\pi} f_k(\sqrt{v_1^2+v'^2-2v_1v'\cos\theta}) d(\sin^2\theta). \tag{11}$$

Here $\alpha_k=(I_k/2m)^{1/2}$ and $v'=v_1-v_2$, where v_1 and v_2 are the projectile and target electron velocities relative to the laboratory, respectively. $f_k(|\mathbf{v}_1-\mathbf{v}'|)=f_k(|\mathbf{v}_2|)$ is the velocity distribution of the electrons in orbital ''k'' *relative to the projectile*.

Concerning the calculation of orbital mean excitation energies (I_k) within the OLPA, Meltzer *et al.* [38] have refined the original treatment based on this scheme [36] making a physically more consistent orbital-by-orbital generalization of the local plasma approximation. From their study, the following expression for the OLPA treatment of I_k is recommended:

$$\ln I_k=\frac{1}{\omega_k}\int_\Gamma \rho_k(\mathbf{r})\ln\left[\hbar\left(\frac{4\pi e^2\rho(r)}{m}\right)^{1/2}\right] d^3\mathbf{r}, \tag{12}$$

where $\rho_k(\mathbf{r})$ is the local electronic density for orbital k and $\rho(r)$ the local total electron density obtained after taking the angular average of each orbital charge density. As before, Γ in Eq. (12) indicates the different domains of integration for the interior and exterior densities.

Strictly speaking, the term $\rho(r)$ in Eq. (12) should include the multiplying scaling parameters, χ_k, for each orbital symmetry, i.e., $\rho(r)=\Sigma_k\chi_k\rho_k(r)$, to account for polarization effects as originally proposed by Lindhard and Scharff [19]. However, the orbital dependence of χ_k is still an open and difficult question to answer. Meltzer *et al.* considered this situation for atomic s and p orbitals and found Eq. (12), with $\chi_k=1$, to be the most reasonable choice for calculating stopping cross sections through the OLPA implementation of the kinetic theory. It is thus reasonable to follow this recommendation and use Eq. (12) as the relevant expression to calculate I_k, in contrast with what was done in Refs. [16] and [36].

Clearly, from Eqs. (11) and (12), the orbital velocity distribution $f_k(\nu,\nu',\theta)$ and charge density $\rho_k(\mathbf{r})$ are important input quantities which must carry the information on the physical conditions of our target system. In the case of a condensed medium subject to pressure, it is clear also that the electronic density will be a function of pressure through the radius of the confining box. The velocity distribution $f_k=|\Phi(k)|^2$ in Eq. (11) may then be obtained with $k=(m/\hbar)\times(v_1^2+v'^2-2v_1v'\cos\theta)^{1/2}$ and with $\Phi(k)$ the Fourier transform of Eqs. (7) and (8), i.e.,

$$\Phi(k)=(2/\pi)^{1/2}[N^i\Omega(k,a,b,R_c)+N^o\Xi(k,g,R_c)], \tag{13a}$$

with the definitions

$$\Omega(k,a,b,R_c)=\frac{\pi^{1/2}}{4a^{3/2}}e^{-k^2/4a}\,\mathrm{Re}\left[\mathrm{erf}\left(R_c\sqrt{a}+i\frac{k}{2\sqrt{a}}\right)\right] - \frac{e^{-aR_c^2}}{2a}R_c j_0(kR_c)-\frac{e^{-bR_c^2}}{k}R_c^2 j_1(kR_c) \tag{13b}$$

and

$$\Xi(k,g,R_c)=\left(\frac{\pi^{1/2}}{4g^{3/2}}\left\{1-\mathrm{Re}\left[\mathrm{erf}\left(R_c\sqrt{g}+i\frac{k}{\sqrt{g}}\right)\right]\right\} + \frac{R_c}{2g}j_0(kR_c)\right)e^{-k^2/4g}, \tag{13c}$$

where N^o,N^i, and the orbital parameters (a,b,g) are defined by Eqs. (7) and (8). erf(z) is the error function of the complex argument and j_0,j_1 are the spherical Bessel functions of order 0 and 1, respectively [39].

Incorporating the above results into Eqs. (9)–(12), the proton electronic stopping cross section may be calculated as a function of target density (pressure). The mean excitation energy, $\langle I\rangle$ [Eq. (12)], was calculated numerically using the optimized orbital parameters for a given confinement (density) condition. Figure 2(b) shows the results of this calculation for $V_B=0$ (continuous curve) and $V_B=\infty$ (chain curve). A continuous increase of $\langle I\rangle$ as the density of the medium increases is observed. This is expected since as density increases, the molecular confinement region is reduced with the consequent compaction of the electron cloud with increasing electron kinetic energy and energy-level shift towards higher values. Once again, the exaggeration of this effect by the hard-wall case is apparent. This behavior has as a direct consequence the reduction in the electronic stopping cross section, as may be verified from Fig. 3, where S_e is plotted against proton velocity for different compression (density) conditions in molecular hydrogen. All these quan-

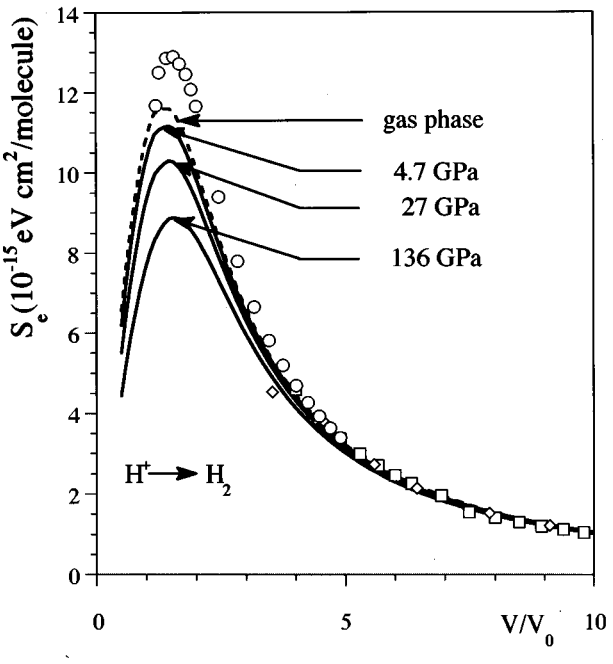

FIG. 3. Electronic stopping cross section for protons incident on dense molecular hydrogen under different pressures as a function of projectile velocity. The gas-phase calculations are shown for comparison. Also shown are gas-phase experiments (○) Ref. [40], (□) Ref. [41], (◇) Ref. [42].

tities were obtained with the soft-wall confinement ($V_B = 0$) model proposed in this work. The experimental points correspond to gas-phase measurements from various authors [40–42] and are included here as a reference. The theoretical predictions for the gas phase using the OLPA/FSGO approach [16] correspond to the dashed curve. In what follows, we shall refer to the latter theoretical results to compare with the predictions of this work for the condensed phase. We first note (not shown in the figure) an almost negligible change (about 0.5%) in S_e for the low-density liquid phase (0.036 mol/cm^3 at 1 atm, 0.0001 GPa, and 20 K) as compared to the gas phase. A similar behavior is expected for the solid phase in the same temperature and pressure conditions. At higher pressures, $P=0.6$ GPa (0.062 mol/cm^3), 4.7 GPa (0.099 mol/cm^3), 27 GPa (0.171 mol/cm^3), and 136 GPa (0.380 mol/cm^3), the maximum predicted differences are, respectively, 1% (not shown), 4%, 11.5%, and 24% below the gas phase. According to Holzapfel [43], fluid molecular hydrogen may be observed for pressures from 10^{-4} GPa ($T \geqslant 20$ K) and by increasing temperature and pressure up to about 100 GPa ($T \geqslant 1000$ K). Solid molecular hydrogen exists below the transition curve connecting the above P-T extreme points. Since thermal effects in S_e are negligible for this range of temperatures [44], the above predicted differences in S_e are common for liquid and solid molecular hydrogen with the same density. Our results for 136 GPa should be viewed as an extrapolation of the density dependence of S_e and would correspond to highly compressed molecular hydrogen in the solid phase ($T<1000$ K) or the metallic fluid ($T>1000$ K).

Unfortunately, there is no experimental information available on proton stopping cross sections in dense molecular hydrogen to corroborate the density effects predicted in this work. In practice, it would be more feasible to perform an experiment in the low-temperature regime for increasing pressures for the solid phase.

IV. DISCUSSION AND CONCLUSIONS

The present work merges two aspects which need particular consideration. First, the molecular confinement model provides a reasonable description of the pressure (density) effect on the properties of molecules in condensed matter. The model with soft walls as applied to the simplest molecular system, the hydrogen molecule, using a single Gaussian representation, has provided new important physical information on the effect of confinement on the H_2 electronic properties. It also provides a cold pressure which correlates properly with a realistic situation for the 0-K isotherm of molecular hydrogen under compression. This is a significant improvement over the hard-wall model, which overestimates the pressure-density behavior, and suggests the use of a realistic molecular wave function to improve the quantitative agreement.

On the other hand, the molecular confinement model proposed in this work is concomitant to the calculation of density effects on the electronic stopping cross section since it considers self-consistently the changes in molecular electronic structure and molecular conformation as the medium density changes. This is important because the inelastic energy loss is directly correlated to the electronic properties of the target (for a bare projectile, as in our case). Hence, the use of a confinement model to account for physical state effects on S_e, whereby the electronic distribution is only renormalized within the effective molecular volume—as was done in Refs. [17] and [18]—may be misleading.

The results of this work for proton stopping in dense molecular hydrogen predict a very small to moderate reduction in S_e relative to the gas phase in going from atmospheric pressure ($\Delta S_e \approx 0.5\%$) up to 136 GPa ($\Delta S_e \approx 24\%$) for either the solid or liquid phase with the same density, depending on the temperature defined by the phase diagram. In spite of the small changes in S_e predicted for this system, it is worthwhile to analyze within the model proposed here the density effect on larger molecular systems for which noticeable physical state effects in S_e have been observed experimentally [1–4]. Work is currently in progress in this direction.

In summary, we have shown here that the target density dependence of the electronic stopping cross section is due to the combined effect of spatial confinement as well as an increase in target mean excitation energy. In contrast with previous confining models to account for phase effects in S_e, we have made a self-consistent treatment of electronic and nuclear redistribution as a function of the degree of confinement and found that the boxed-in-molecule model within soft walls gives a more realistic description for the pressure-density dependence of the condensed phase than the hard-wall model. The proposed model is of a general character and may be applied to molecules of arbitrary size and symmetry.

ACKNOWLEDGMENT

We are grateful to R. Cabrera-Trujillo for valuable discussions during the early stages of development of this work.

APPENDIX

As stated in the main text, for $V_B=\infty$ the exterior wave function [Eq. (7b)] vanishes ($g\rightarrow\infty$) and the interior wave function becomes ($a=b$)

$$\Psi^i(r)=N(e^{-ar^2}-e^{-aR_c^2}), \tag{A1}$$

with N given as

$$N=[f(a,R_c)+g(a,R_c)]^{-1/2}, \tag{A2a}$$

where

$$f(a,R_c)=(3/a+4R_c^2/3)\pi R_c e^{-2aR_c^2} \tag{A2b}$$

and

$$g(a,R_c)=(\pi/a)^{3/2}[2^{-3/2}\,\mathrm{erf}(R_c\sqrt{2a})-\mathrm{erf}(R_c\sqrt{a})e^{-aR_c^2}], \tag{A2c}$$

with erf(z) the error function [39].

The following expressions for the one-electron kinetic energy as well as the electron-nuclear attraction terms are obtained:

$$\langle 1|-\tfrac{1}{2}\nabla^2|1\rangle=(\pi N^2/2)\left[\frac{3}{2}\left(\frac{\pi}{2a}\right)^{1/2}\mathrm{erf}(R_c\sqrt{2a})-(3+4aR_c^2)R_c e^{-2aR_c^2}\right], \tag{A3}$$

$$\left\langle 1\left|\frac{1}{|\mathbf{r}-\mathbf{R}_N|}\right|1\right\rangle=(\pi N^2/3a)[\kappa(a,R_c,R_N)-\lambda(a,R_c,R_N)], \tag{A4}$$

with

$$\kappa(a,R_c,R_N)=(9+6aR_c^2-2aR_N^2)e^{-2aR_c^2} \tag{A5a}$$

and

$$\lambda(a,R_c,R_N)=\frac{6}{R_N}\left(\frac{\pi}{a}\right)^{1/2}\mathrm{erf}(R_N\sqrt{a})e^{-aR_c^2}+\frac{3}{2R_N}\left(\frac{\pi}{2a}\right)^{1/2}\mathrm{erf}(R_N\sqrt{2a}), \tag{A5b}$$

where R_N is half the internuclear distance and N given by Eqs. (A2).

Analogously, the two-electron Coulomb and exchange term [Eq. (5b)] becomes

$$(11|11)=(\pi^2N^4/60a^{5/2})[\mu(a,R_c)+\eta(a,R_c)], \tag{A6}$$

with

$$\mu(a,R_c)=8a^{1/2}R_c(15+60aR_c^2+16a^2R_c^4)\times e^{-4aR_c^2}-480\pi^{1/2}(1+aR_c^2)\mathrm{erf}(R_c\sqrt{a})e^{-3aR_c^2} \tag{A7a}$$

and

$$\eta(a,R_c)=10\left(\frac{\pi}{2}\right)^{1/2}(63+12aR_c^2)\mathrm{erf}(R_c\sqrt{2a})e^{-2aR_c^2}-240\left(\frac{\pi}{3}\right)^{1/2}\mathrm{erf}(R_c\sqrt{3a})e^{-aR_c^2}+15\pi^{1/2}\,\mathrm{erf}(2R_c\sqrt{a}). \tag{A7b}$$

For $V_B=0$, the interior and exterior wave functions are equal, hence $b\rightarrow\infty$ and $a=g$ in Eqs. (7a) and (7b), i.e.,

$$\Psi^i(r)=\Psi^e(r)=N_0e^{-ar^2}, \tag{A8}$$

with $N_0=(2a/\pi)^{3/4}$. The corresponding one-electron kinetic energy, electron-nuclear attraction, and two-electron terms are easily evaluated in this case and are, respectively,

$$\langle 1|-\tfrac{1}{2}\nabla^2|1\rangle=3a/2, \tag{A9}$$

$$\left\langle 1\left|\frac{1}{|\mathbf{r}-\mathbf{R}_N|}\right|1\right\rangle=\mathrm{erf}(R_c\sqrt{2a})/R_N-(8a/\pi)^{1/2}e^{-2aR_c^2}, \tag{A10}$$

$$(11|11)=(8aR_c/\pi)e^{-4aR_c^2}+(4a/\pi)^{1/2}\mathrm{erf}(2R_c\sqrt{a})-(32a/\pi)^{1/2}\mathrm{erf}(R_c\sqrt{2a})e^{-2aR_c^2}. \tag{A11}$$

[1] D. I. Thwaites, Radiat. Res. **95**, 495 (1983).
[2] D. I. Thwaites, Nucl. Instrum. Methods Phys. Res. B **12**, 84 (1985).
[3] D. I. Thwaites, Nucl. Instrum. Methods Phys. Res. B **27**, 293 (1987).
[4] D. I. Thwaites, Nucl. Instrum. Methods Phys. Res. B **69**, 53 (1992).
[5] P. Bauer, W. Rössler, and P. Mertens, Nucl. Instrum. Methods Phys. Res. B **69**, 46 (1992).
[6] P. Bauer, R. Golser, D. Semrad, P. Maier-Komor, F. Aumayr, and A. Arnau, Nucl. Instrum. Methods Phys. Res. B **136/138**, 103 (1998), and references therein.
[7] J. R. Sabin and J. Oddershede, Nucl. Instrum. Methods Phys. Res. B **64**, 678 (1992).

[8] E. K. L. Chau, D. Powers, A. S. Lodhi, and R. B. Brown, J. Appl. Phys. **49**, 2346 (1978).
[9] J. F. Ziegler and J. M. Manoyan, Nucl. Instrum. Methods Phys. Res. B **35**, 215 (1988).
[10] R. Kreutz, W. Neuwirth, and W. Pietsch, Phys. Rev. A **22**, 2598 (1988).
[11] J. R. Sabin and J. Oddershede, Nucl. Instrum. Methods Phys. Res. B **27**, 280 (1987).
[12] J. Oddershede and J. R. Sabin, Nucl. Instrum. Methods Phys. Res. B **42**, 7 (1989).
[13] S. A. Cruz and J. Soullard, Nucl. Instrum. Methods Phys. Res. B **61**, 433 (1991); **71**, 387 (1992).
[14] J. Soullard, S. A. Cruz, and R. Cabrera-Trujillo, Nucl. Instrum. Methods Phys. Res. B **80/81**, 20 (1993).
[15] S. A. Cruz, J. Soullard, and R. Cabrera-Trujillo, Nucl. Instrum. Methods Phys. Res. B **83**, 5 (1993).
[16] R. Cabrera-Trujillo, S. A. Cruz, and J. Soullard, Nucl. Instrum. Methods Phys. Res. B **93**, 166 (1994).
[17] Y. J. Xu, G. S. Khandelwal, and J. W. Wilson, Phys. Rev. A **32**, 629 (1985).
[18] G. Both, R. Krotz, K. Lohmer, and W. Neuwirth, Phys. Rev. A **28**, 3212 (1983).
[19] J. Lindhard and M. Scharff, K. Dan. Vidensk. Selsk. Mat. Fys. Medd. **27**, No. 15, (1953).
[20] E. Ley-Koo and S. A. Cruz, J. Chem. Phys. **74**, 4603 (1981).
[21] R. LeSar and D. R. Herschbach, J. Phys. Chem. **85**, 2798 (1981); **87**, 520 (1983).
[22] J. Gorecki and W. Byers-Brown, J. Chem. Phys. **89**, 2138 (1988).
[23] J. L. Marin and G. Muñoz, J. Mol. Struct.: THEOCHEM **287**, 281 (1993).
[24] T. Pang, Phys. Rev. A **49**, 1709 (1994).
[25] A. A. Frost, Theor. Chim. Acta **18**, 156 (1970), and references therein.
[26] H. M. James and A. S. Coolidge, J. Chem. Phys. **1**, 825 (1933).
[27] S. A. Cruz, J. Soullard, and E. G. Gamaly (unpublished).
[28] M. Moshinsky and Y. Smirnov, *The Harmonic Oscillator in Modern Physics*, in Contemporary Concepts in Physics Vol. 9 (Harwood Academic, Amsterdam, 1996), pp. 29–43.
[29] G. I. Kerley, in *Molecular-Based Study of Fluids*, edited by J. M. Haile and G. A. Mansoori (American Chemical Society, Washington, D.C., 1983), pp. 107–138.
[30] W. J. Evans and I. F. Silvera, Phys. Rev. B **57**, 14 105 (1998).
[31] R. J. Hemley, H. K. Mao, L. W. Finger, A. P. Jephcoat, R. M. Hazen, and C. S. Zha, Phys. Rev. B **42**, 6458 (1990).
[32] J. Gorecki and W. Byers-Brown, J. Phys. B **21**, 403 (1988).
[33] P. Loubeyre, R. Le Toullec, D. Hausermann, M. Hanfland, R. J. Hemley, H. K. Mao, and L. W. Finger, Nature (London) **383**, 702 (1996).
[34] I. F. Silvera, Rev. Mod. Phys. **52**, 393 (1980).
[35] H. K. Mao and R. J. Hemley, Rev. Mod. Phys. **66**, 671 (1994).
[36] D. E. Meltzer, J. R. Sabin, and S. B. Trickey, Phys. Rev. A **41**, 220 (1990), **42**, 666(E) (1990).
[37] J. Oddershede and J. R. Sabin, Int. J. Quantum Chem., Quantum Chem. Symp. **23**, 557 (1989).
[38] D. E. Meltzer, J. R. Sabin, S. B. Trickey, and J. Z. Wu, Nucl. Instrum. Methods Phys. Res. B **82**, 493 (1993).
[39] M. Abramowitz and I. A. Stegun, *Handbook of Mathematical Functions* (Dover, New York, 1972).
[40] H. K. Reynolds, D. N. F. Dunbar, W. A. Wenzel, and W. Whaling, Phys. Rev. **92**, 742 (1953).
[41] H. Bichsel and L. E. Porter, Phys. Rev. A **25**, 2499 (1982).
[42] R. A. Langley, Phys. Rev. B **12**, 3575 (1975).
[43] W. B. Holzapfel, Rep. Prog. Phys. **59**, 29 (1996).
[44] J. R. Sabin, J. Oddershede, and I. Paidarova, Nucl. Instrum. Methods Phys. Res. B **93**, 161 (1994).